(28) B. Longato, F. Morandini, and S. Bresadola, *J. Organomet. Chem.*, **88**, C7 (1975).
(29) M. G. Clerici, S. Di Gioacchino, F. Maspero, E. Perrotti, and A. Zanobi, *J. Organomet. Chem.*, **84**, 379 (1975).
(30) C. T. Enos, G. L. Geoffroy, and T. H. Risby, *Anal. Chem.*, **48**, 990 (1976).
(31) For other examples, see ref 19.
(32) M. J. Mays, R. N. F. Simpson, and F. P. Stefanini, *J. Chem. Soc. A*, 3000 (1970).
(33) G. S. Arnold, W. L. Klotz, W. Halper, and M. K. DeArmond, *Chem. Phys. Lett.*, **19**, 546 (1973).
(34) A. P. Ginsberg and B. K. Teo, presented at the 169th American Chemical Society National Meeting, Philadelphia, Pa., April 1975.
(35) B. K. Teo, A. P. Ginsberg, and J. C. Calabrese, *J. Am. Chem. Soc.*, **98**, 3027 (1976).
(36) A. P. Ginsberg, private communication.
(37) Estimated from data given by L. Vaska and M. F. Werneke, *Trans. N.Y. Acad. Sci.*, **33**, 70 (1971).

Applications of X-Ray Photoabsorption Spectroscopy to the Determination of Local Structure in Organometallic Compounds

S. P. Cramer, T. K. Eccles, F. Kutzler, Keith O. Hodgson,* and S. Doniach*

Contribution from the Department of Chemistry and Department of Applied Physics, Stanford University, Stanford, California 94305. *Received February 6, 1976*

Abstract: Curve fitting methods have been developed which promise to be of considerable utility in extracting structural information from x-ray absorption spectra. In principle, the extended x-ray absorption fine structure (EXAFS) for a given atom can be analyzed to reveal the radial distances and atomic numbers of those atoms surrounding the absorber. The requisite high-quality x-ray absorption spectra can now be easily and rapidly obtained on solid or solution samples, using synchrotron radiation from the Stanford electron-positron storage ring SPEAR at the Stanford Linear Accelerator Center. In order to provide the basis for an understanding of metalloprotein absorption fine structure, data for ferrocene, $Co(NH_3)_6^{3+}$, $Co(OH_2)_6^{2+}$, and a variety of iron porphyrins have been analyzed. The procedure used was to fit the EXAFS of known structures with a parameterized, semiempirical function: $\sum_i C_i k^{-\beta_i} \exp(-2\langle\sigma_i^2\rangle k^2) \sin(2R_i k + \alpha(k))$; where the sum is over all neighboring atoms, the distance information R_i is contained in the phase term, and the other variables account for the amplitude behavior as described in detail in the text. These parameters are then used in fits on other known structures, and the accuracy of the calculated distances (R_i) is used as a test for the validity of the method. The results of fits on $Fe^{II}TPP$, $Fe^{III}TPP(SC_6H_5)$, and FeTpivPP(N-MeIm)O_2 indicate that radial distances out to four coordination shells in iron porphyrins can be determined to better than 0.1 Å. For cases where the interest is only in changes in coordination, difference methods of analysis have been developed which allow accurate determination of the geometry and distances to small molecules such as dioxygen which can reversibly bind to the metal ion. For oxy and deoxy FeTpivPP(N-MeIm), the Fe-O distances are determined to better than 0.03 Å. At present, the interpretation of the EXAFS from an unknown structure relies heavily on comparison with model compound data. However, the present results suggest that a library of transferable phase shift and amplitude functions may be eventually compiled, and that curve-fitting analysis of the extended fine structure will be useful for determining the local structure around specific atomic constituents in metalloproteins and other complex materials.

The recent availability of a stable, intense x-ray source using synchrotron radiation from high energy (GeV) electron storage rings[1] has generated a renaissance of interest in x-ray absorption spectroscopy. Following the absorption edge, where the photon energy equals the binding energy of a core electron, simple models of x-ray photoabsorption predict a gradual monotonic decrease in the absorption coefficient with increasing photon energy.[2] Although such behavior is approximately observed for noble gas spectra, the presence of other atoms around the absorber causes the appearance of a periodic modulation in the absorption coefficient. This modulation contains information about the nature of the surrounding atoms and their distances to the absorber. The absorption coefficient oscillations have been termed EXAFS (Extended X-ray Absorption Fine Structure) or alternatively Kronig structure, and until recently they were more a theoretical curiosity than a useful structural tool.[3] It is the purpose of this paper to illustrate the application of x-ray absorption spectroscopy to the study of the local environments around specific metal centers in complex molecules. Specifically, in an earlier communication[4] we suggested that x-ray absorption spectroscopy might be useful for structural investigation of molecules such as metalloporphyrins. We consider herein detailed application of this method to the study of the molecular environment of the iron in porphyrins.

While it is easy to show that the extended fine structure is related to the radial distribution of atoms around the absorbing atom, there is considerable difficulty in interpreting the data in a quantitative manner. The extended fine structure was first treated theoretically by Kronig in the 1930's.[5] More recent theoretical treatments of EXAFS by Ashley and Doniach,[6] Lee and Pendry,[7] and Sayers and Stern[8] have emphasized the effect of short-range photoelectron backscattering on the transition probabilities to the continuum states. Multiple scattering effects have also been treated by these authors. While theoretical calculations cannot as yet produce perfect agreement with experimental results, they provide a useful foundation upon which to base empirical methods.

Since EXAFS is essentially a result of the photoelectron backscattering from the surrounding atoms, it contains information about the nature of these atoms and their distances from the absorbing atom. Unfortunately, this information is veiled by the energy dependence of the electron-atom backscattering function. Inelastic processes may also complicate the fine structure. Recent attempts to unravel the structural information from EXAFS have involved three types of approaches: (1) ab initio calculations, (2) Fourier transformation, and (3) curve-fitting.

Using a short-range-order electron-atom backscattering approach as a starting point, Kincaid and Eisenberger[9] have

attempted to calculate an EXAFS spectrum ab initio for Br_2 and $GeCl_4$ vapors. Electron-atom scattering amplitudes and phase shifts were calculated by numerically integrating Schrodinger's equation. Using the bond lengths and strengths obtained from vibrational spectroscopy and electron diffraction, they then calculated theoretical EXAFS spectra and compared the results with the experimental data. Although agreement was obtained to within 5% for the phase of the scattering, quantitative disagreement beyond experimental error was observed for the amplitude. The results suggest that the basic theory of the extended fine structure is correct as far as elastic scattering goes, but that ab initio calculation of spectra will also have to include inelastic effects.

A Fourier transform analysis procedure has been used extensively by Sayers, Stern, and Lytle to study the short range order of amorphous materials.[10] Comparison of the extended fine structure of amorphous and crystalline germanium clearly shows the decrease in order beyond the first coordination sphere in amorphous Ge. Similar results are observed with amorphous vs. crystalline GeO_2. Fourier transform analyses have been carried out on a copper porphyrin.[11a] Sayers, Stern, and Lytle have also exploited the temperature dependence of the extended fine structure to obtain mean square deviations in atom–atom distances, and they use their methods for estimating coordination numbers, electron-scattering amplitudes, and photoelectron mean free paths.[11b,c]

The curve fitting methods reported here represent an alternative approach for obtaining quantitative information from extended fine structure data. We recognize that both the phase and amplitude of the fine structure modulation may be photoelectron energy dependent functions. We use a minimization curve-fitting technique to fit the observed spectra of known compounds to a semiempirical formula, expressed in terms of a limited number of parameters. These parameterized functions may then be applied to curve fitting spectra of other compounds, leading ultimately to the solution of unknown structures.

Related methods of analysis are being developed independently by Shulman, Eisenberger, Blumberg and Stambaugh.[12] Using iron–sulfur phase shifts derived from model compounds, they fitted data on lyophilized, oxidized rubredoxin with a nine-parameter amplitude function. A statistical analysis of the phase of the fine structure revealed that the Fe–S distances were very close, if not equivalent.

The results reported in the present paper suggest that by using our approach to compare spectra of closely related compounds, precise and reliable distance information may be obtained about the environment of the absorbing atom, out to a distance of 4–5 Å.

Both phase-shift and amplitude functions appear to be transferable between similar compounds. Finally, the fine structure for a complicated molecule may be approximated as the sum of contributions from the individual atoms. This additivity of EXAFS is essentially a neglect of multiple and inelastic scattering processes, and such an approximation appears valid when the absorber is surrounded by low Z scattering atoms, none of which are obscured from direct interaction with the absorber.

Experimental Section

Materials. All materials were prepared according to literature methods. *meso*-Tetraphenylporphyriniron(II), Fe(TPP), was prepared by the method of Collman et al.[13] *meso*-Tetraphenylporphyrinbis(*N*-methyl(imidazole))iron(II), Fe(TPP)(N-Me(imid))$_2$, was obtained from Fe(TPP) by the method of Collman and Reed.[14] *meso*-Tetraphenylporphyrinbis(imidazole)iron(III) chloride, Fe(TPP)(imid)$_2$Cl, was prepared by the method of Epstein, Straub, and Maricondi.[15] The sulfur liganded porphyrin, *meso*-tetraphenylporphyrin(benzenethiolato)iron(III), Fe(TPP)(SC_6H_5), was prepared by the method of Collman, Sorrell, and Hoffman.[16] Reagent grade hemin chloride, Fe(PPIX)Cl, was purchased from Fluka AG.

The "oxy picket fence porphyrin", dioxygen[mono-*N*-methylimidazole-*meso*-tetra($\alpha,\alpha,\alpha,\alpha$-*O*-pivalamidophenyl)porphyrin]iron(II), Fe($\alpha,\alpha,\alpha,\alpha$-TpivPP)(N-Me(imid))$O_2$, was a generous gift from Professor J. P. Collman of the Stanford Chemistry Department. The deoxygenated analogue of this porphyrin Fe($\alpha,\alpha,\alpha,\alpha$TpivPP)(N-Me(imid)) was prepared as described by Collman[17] by deoxygenation of the solid oxygenated porphyrin at 68 °C for 18 h. The deoxygenation reaction was monitored by recording the solution spectra in the uv and visible regions. Ferrocene[18] and $Co(NH_3)_6Cl_3$[19] were also prepared by standard procedures.

X-Ray Absorption Measurements. All x-ray absorption spectra were recorded using radiation from the Stanford Positron Electron Accelerating Ring (SPEAR) and the facilities of the Stanford Synchrotron Radiation Project, SSRP, a national facility for the exploitation of synchrotron radiation.[20] The measurements were made using an apparatus originally constructed by Kincaid, Eisenberger, and Sayers which has been described in detail elsewhere.[21] In essence, the synchrotron radiation is defined by slits and monochromated by a Si(220) channel cut single crystal. The monochromatic 1 × 20 mm x-ray beam passes through one ion chamber to measure incident intensity (I_0), then goes through the sample, and finally through a second ionization detector which measures transmitted intensity (I). The ratio I/I_0 is recorded as a function of monochromator angle by means of an interfaced PDP 11/05 computer.

Porphyrin samples were measured as solid pellets approximately 0.1 mm thick. Ferrocene, $Co(NH_3)_6Cl_3$, and $CoCl_2 \cdot 2H_2O$ were run as 1 M solutions, the former in benzene, the latter two in water. The porphyrin spectra reported herein were typically recorded with 1 s per point integration with steps being taken approximately every 1 eV beginning around 50 eV below the absorption edge to around 600 eV above the edge. Lack of any detectable sample decomposition was demonstrated by recording the x-ray absorption spectra of the same sample repeatedly during a period of several hours. For example, with Fe($\alpha,\alpha,\alpha,\alpha$-TpivPP)(N-Me(imid))$O_2$, no detectable changes were observed in the spectra during repeated measurements of the same sample over a 4-h period.[22] The deoxy picket fence porphyrin was prepared as described above and transferred into a gas-tight cell with Kapton windows in an inert atmosphere box. The cell was stored under argon until just prior to recording the spectrum.

Numerical Analysis Methods. The numerical calculations described in this paper were performed on a PDP 11/45 computer with 28 K of core and a floating point processor. The calculations routinely involved Fourier transforms and minimization programs which were tailored for use by the small computer.[23]

Least absolute value refinements were used rather than least squares because they converged much more rapidly. Several least-squares refinements were done, however, and these showed that the constants arrived at by each method for the same fit were within one standard deviation of each other. The only difference in the programming between the two methods was the substitution of absolute value for the value squared in the function to be minimized.

The errors were estimated from the variance by established procedures. For example, the error in the jth parameter, σ_j, obtained by the fitting procedure was estimated by:

$$\sigma_j = \left\{ \left[\frac{1}{N-n} \sum_{i=1}^{N} k^3(\chi_i - F_i)^2 \right] \alpha_{jj}^{-1} \right\}^{1/2}$$

where N is the number of data points used in the fit, n the number of parameters adjusted, χ_i and F_i a data point value and its corresponding value of the fitting function, and α_{jj}^{-1} a diagonal element of the inverse matrix of normal equations weighted by k^3.

The Fourier transform program was used in both Fourier filtering and in actual data analysis as described in the next section of this paper. The real and imaginary components of the Fourier transform were obtained using the following formulas:

$$\phi_{\text{real}}(nR_{\text{inc}}) = \frac{2R_{\text{inc}}}{\pi} \int_{k_i}^{k_f} k^3 \chi(k) \cos(2nR_{\text{inc}}k)\, dk$$

$$\phi_{\text{imag}}(nR_{\text{inc}}) = \frac{2R_{\text{inc}}}{\pi} \int_{k_i}^{k_f} k^3 \chi(k) \sin(2nR_{\text{inc}}k)\, dk$$

where n is an integer and R_{inc} is the distance between points in R space, and $\chi(k)$ is the value of the normalized fine structure. The integrations for the Fourier transforms were done numerically by

Simpson's rule. The modulus of the Fourier transform (which is plotted in the transforms in this paper) is obtained by the formula $\phi_{mod} = (\phi_{real}^2 + \phi_{imag}^2)^{1/2}$.

The Simpson's rule integrations also made it possible to include a quadratic term in the transform, that is cos $(2nR_{inc}k + Ck^2)$. However, the investigation of the effect of this extra term was not pursued extensively.

Data Reduction

For the purpose of data analysis, it is necessary to obtain normalized fine structure as a function of photoelectron wave vector in Å^{-1} ($k = \sqrt{0.262\,467(E - E_{edge})}$ eV). In order to plot the fine structure as a function of wave vector, an edge position must first be defined. To determine this position, the x-ray absorption data are plotted as log (I_0/I) (absorbance) vs. energy, along with the first and second derivative curves. Figure 1 shows data from the oxy "picket fence" porphyrin, Fe($\alpha,\alpha,\alpha,$-TpivPP)(N-Me(imid))(O_2), and the first derivative of these data. The derivative curves are calculated by fitting a polynomial to five points on either side of each individual point and differentiating the polynomial. Such curves are useful in determining the positions of peaks and inflection points of the edges. For the purposes of this paper the edge energy was usually defined as the energy of the highest inflection point. Errors of up to 5 eV in edge position as defined in this manner will fall to within <5% in assigning the k value for $k > 3.6$ Å^{-1}.

Obvious glitches in the x-ray absorption data can be removed where necessary by fitting a polynomial over a certain range and replacing the data values with the polynomial values. Such procedures are normally necessitated by the fact that rapid changes in incident x-ray intensity occur at angles where the 220 monochromating crystal has other resonances. Following this procedure, the data are converted to absorbance vs. wave vector k and arbitrarily normalized so that the absorbance values always fall between 0 and 1. The absorption data must then be converted to fine structure. This can be accomplished by fitting a polynomial (of order from 1 to 3) over some range of the absorption curve, and subtracting it from the data.[25] One of the main problems in "background subtraction" is that this background represents atomic absorption in the absence of neighbors. Since data for the absorption in the absence of neighbors are not normally available, the correction for background remains somewhat arbitrary.

Another background subtraction scheme used Fourier filtering[11b,c] of the data with respect to k after the polynomial subtraction. Fourier filtering is accomplished by Fourier transforming the data into R space, selecting the R range to be kept, and retransforming to k space. The Fourier filtering can be used to remove large peaks in the R range of 0 to 1 Å whose position and height vary as a function of the background polynomial fitting range and order. Peaks in the transform above 1 Å did not show this variation, and thus the peaks below 1 Å were attributed to residual background. As significant peaks in the Fourier transforms generally come below R of 5 Å, a high frequency cutoff of 7 Å is reasonable. Figure 2 shows a comparison between filtered and unfiltered data for Fe($\alpha,\alpha,\alpha,\alpha$-TpivPP(N-Me(imid))$O_2$ in which the filtered data were Fourier transformed to R space, cut off below R of 0.5 Å and above R of 7.0 Å, and retransformed to k space. In addition to eliminating low frequency drift of the baseline, reduction in the high frequency noise is clearly visible. Figure 3 shows the actual background line subtracted by each method. The possible effects of cutoff errors introduced by the transform operation itself are considered later by comparing numerical results on the same data set for both filtered and unfiltered data. In essence, at values of $k \geq 4$ Å where the fitting is normally done, the simple polynomial scheme and unfiltered data worked very well for the porphyrin data analysis.

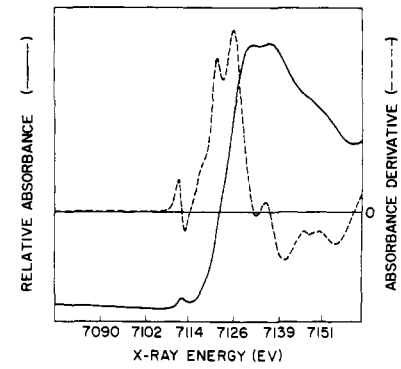

Figure 1. X-Ray absorption spectrum for Fe($\alpha,\alpha,\alpha,\alpha$-TpivPP)(N-Me(imid))$O_2$ in the region of the Fe K absorption edge. The solid line is a plot of the absorbance vs. energy while the dotted line is the first derivative of this curve.

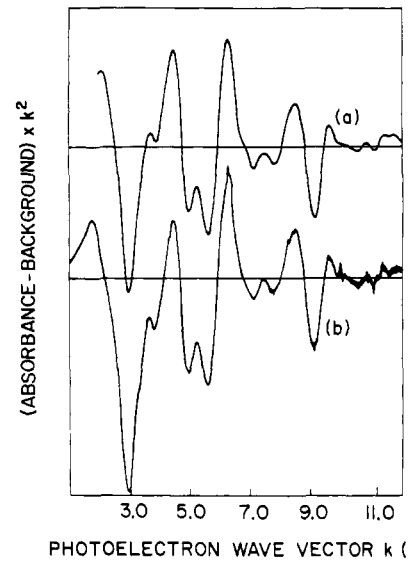

Figure 2. A comparison of filtered (upper curve) and unfiltered (lower curve) extended fine structure spectra for Fe($\alpha,\alpha,\alpha,\alpha$-TpivPP)(N-Me(imid))$O_2$. The filtering was done by transforming the data into R space, cutting off at R of 0.5 and 7 Å, and retransforming to k space.

Methods of Analysis and Results

Numerical Analysis. As expected from the single scattering theory[6a] the energy dependent modulation χ of the x-ray absorption coefficient μ of atom X by an atom Y at distance R_{XY} is given semiempirically by the general expression:

$$\chi(k) \equiv \frac{\mu - \mu_0}{\mu_0} = \frac{1}{kR_{xy}^2} f(\pi,k) \sin(2kR_{xy} + \alpha(k)) e^{-2\langle\sigma^2\rangle k^2}$$

where k is the photoelectron wave vector; $f(\pi,k)$ is the backscattering amplitude of the outgoing electron from a neighbor at distance R_{xy}; $\alpha(k)$ is the total phase shift undergone by an electron leaving the K shell, backscattering, and returning to interfere at the K shell; $\langle\sigma_i^2\rangle$ is the mean square thermal motion along R_{XY}. This expression is expected to be a reasonable approximation at high photoelectron energies, above 50 eV, in which case multiple scattering terms are small and scattering amplitudes are smoothly varying. The crucial functions to know for the present analysis are $f(\pi,k)$ and $\alpha(k)$, since we find that in practice the damping due to thermal motion can be treated by a single parameter and is fairly well understood.

The calculations of Kincaid[26] and others predict that for low

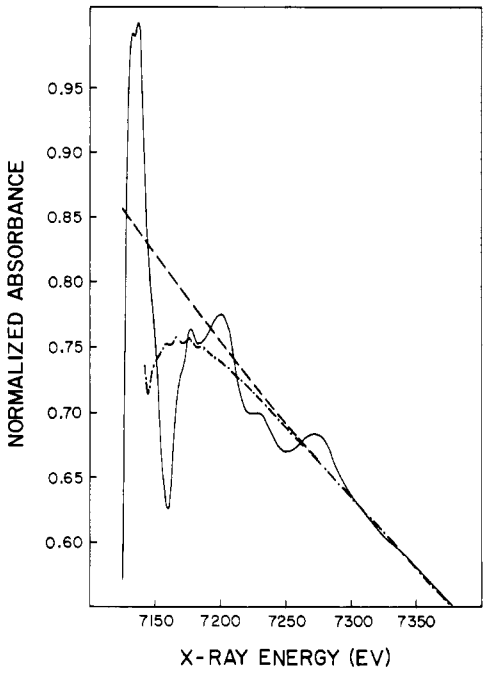

Figure 3. A comparison of the total background removed by two different background subtraction schemes. The solid line shows the absorbance vs. energy spectrum for Fe($\alpha,\alpha,\alpha,\alpha$-TpivPP)(N-Me(imid))$O_2$. The dashed (- - -) line is the background subtraction curve obtained by fitting a third order polynomial over the range of 7200-7350. The other background curve (· · · · · · ·) was obtained by Fourier transforming the data into R space (after the third-order polynomial removal), cutting at R of 0.5 and 7.0 Å, and retransforming into k space.

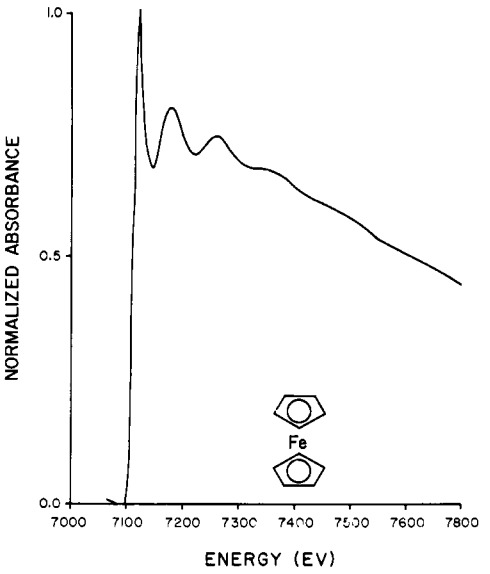

Figure 4. X-Ray absorption spectrum of ferrocene.

Z elements (e.g., C, N, O) the backscattering amplitude should peak below 100 eV and then drop off monotonically. It also appears that the total phase shift will be a smoothly varying function beyond $k = 4$ Å^{-1}. We decided to model the total amplitude behavior by a function based on the form $Ce^{-2\langle\sigma_i^2\rangle k^2}/k^\beta$. The exponential factor approximates the damping due to thermal motion. The factor $1/k^\beta$ in this amplitude function includes the $1/k$ factor from the general expression as well as the backscattering amplitude $f(\pi,k)$.

A quadratic variation is assumed as the model for the total phase shift

$$\alpha(k) = a_0 + a_1k + a_2k^2$$

This gives rise to the following functional form for the extended fine structure:

$$\chi(k) = \sum_i \frac{C_i e^{-2\langle\sigma_i^2\rangle k^2}}{k^\beta i} \sin(2R_ik + a_{0i}k + a_{1i}k + a_{2i}k^2)$$

where the sum over i shells indicates that equivalent atoms at the same distance from the absorber are treated as a group. The distance information is included in the linear term $(2R_i + a_{1i})k$ during the fitting process, for convenience. The distance is then extracted at the end if the linear k dependent term a_{1i} is known.

To test the validity of our functional form, we used data from the solution spectra of ferrocene, $Co(NH_3)_6^{3+}$, and $Co(OH_2)_6^{2+}$. The results of curve fitting this functional form to the data are summarized in Table I.

Single Shell Results. The x-ray absorption spectrum of ferrocene is shown in Figure 4. The inflection point nearest the top of the steep rise occurs at 7126.5 eV and this point was taken as the Fe K absorption edge. The background was removed by fitting a third-order polynomial over the range 7200-7725 eV and subtracting it from the data. The Fourier transform of this data is shown in Figure 5. The data were Fourier filtered by transforming it from the range of 2-12 Å^{-1} and retransforming from the R range 0.5-7 Å. One shell fits were done on both filtered and unfiltered data, and the results of the fits and Fourier transforms are summarized in Table I. The errors shown in parentheses are the estimated standard deviations. Note that when β, a_2, and $2\langle\sigma_i^2\rangle$ are fixed at 2.0, 0.0, and 0.015 respectively, the standard deviation on the remaining constants is much lower, and still shows a consistent $(2R + a_1)$ value. A single shell fit of the ferrocene data is shown in Figure 6. The fit and data shown in this figure have been

Table I. Results of Single Shell Fits on Ferrocene, $[Co(NH_3)_6]^{3+}$ and $[Co(OH_2)_6]^{2+}$

Data set	k range (Å^{-1})	No. of points	$(2R + a_1)$,[a] Å	β_i[b]	a_2	$2\langle\sigma_i^2\rangle$
Ferrocene (unfiltered)	2-12	97	3.40 (21)	2.15 (55)	−0.005 (010)	0.007 (010)
	2-12	97	3.26 (06)	2.0 (0)	0.0 (0)	0.015 (0)
	4-12	98	3.33 (14)	2.13 (45)	0.0008 (0100)	0.010 (5)
	4-12	98	3.33 (02)	2.0 (0)	0.0 (0)	0.015 (0)
Ferrocene (filtered)	2-12	101	3.27 (20)	1.93 (51)	0.004 (18)	0.011 (1)
	2-12	101	3.31 (05)	2.0 (0)	0.0 (0)	0.015 (0)
	4-12	81	3.27 (14)	1.90 (45)	0.005 (10)	0.014 (5)
	4-12	81	3.30 (02)	2.0 (0)	0.0 (0)	0.015 (0)
$[Co(OH_2)_6]^{3+}$ (unfiltered)	4-12	83	3.24 (26)	1.71 (91)	−0.001 (21)	0.028 (12)
	4-12	83	3.26 (04)	2.0 (0)	0.0 (0)	0.015 (0)
$[Co(NH_3)_6]^{3+}$ (unfiltered)	4-12	83	3.15 (18)	1.96 (63)	−0.001 (10)	0.014 (7)
	4-12	83	3.16 (03)	2.0 (0)	0.0 (0)	0.015 (0)

[a] The numbers given in parentheses represent the estimated standard deviation on the numbers in the last digit or digits as so indicated. [b] A standard deviation of zero indicates that the value was fixed in the refinement.

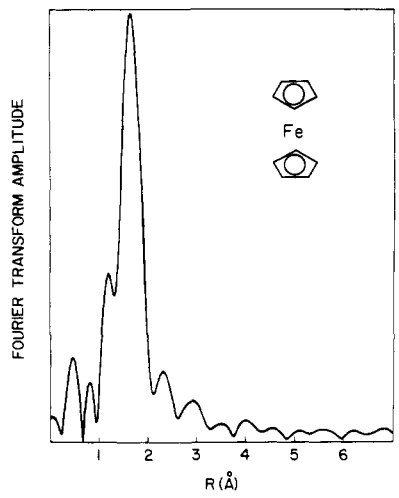

Figure 5. Fourier transform of the ferrocene x-ray absorption data shown in Figure 4 after the background was removed by fitting a third-order polynomial over the range of 7200–7725 eV. The data were transformed over the range of k = 2–12 Å^{-1}.

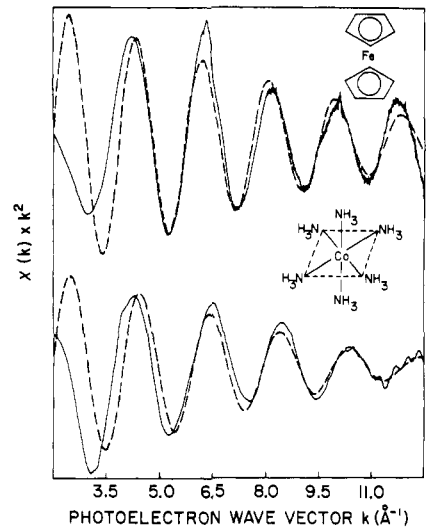

Figure 6. Single shell fits on ferrocene (upper curves) and the $[Co(NH_3)_6]^{3+}$ complex in solution (lower curves). In both cases, the semiempirical function (described in the section on single shell data and the functional form) was fit over the range of k = 4–12 Å^{-1} using unfiltered data. As expected, the functional form does not give good agreement near the edge at low k.

multiplied by k^2 in order to show the goodness of fit in the high k region as well as near the edge. As expected, near the edge the fit is poor since the data were not fitted over this range, and because the single scattering theory is not applicable close to threshold, but it is much better over the k range of 4–12 Å^{-1}. The average $(2R + a_1)$ value from the ferrocene one shell fits of 3.31 Å agrees reasonably well with the value of two times R of 3.36 Å from the ferrocene Fourier transform. This suggests that approximating $\alpha(k)$ as a linear function of k is reasonable, at least over the range of k = 4–12 Å^{-1}. It is also seen that the values of $(2R + a_1)$ are more dependent on the range of fit for the unfiltered data, with the lowest $(2R + a_1)$ value being shifted to a considerably higher value for the fit done using unfiltered data over the range of k = 2–12 Å^{-1}.

The estimated standard deviation of $(2R + a_1)$ as estimated from the variance of all of the different fits of ferrocene in Table I is 0.12 Å. This value agrees well with the values estimated from the fitting routine and together these suggest a limit on the accuracy of the data from this particular analysis of about 0.1 Å.

Using floating exponential factors and quadratic phase shifts, the power of $(1/k)$ in the amplitude function was optimized for ferrocene, $Co(NH_3)_6^{2+}$, and $Co(OH_2)_6^{2+}$. We thus arrived at respective powers of $(1/k)$ of 2.13, 1.96, and 1.71 for β parameters of carbon, nitrogen, and oxygen, respectively. The general trend is for backscattering amplitudes to die out more slowly as the atomic number of the scatterer increases. This is in accord with the predictions of Kincaid based on electron-atom scattering calculations. (These calculations also predict a peak in the scattering amplitude at low photoelectron energies, but our fits begin after the monotonic decline in $|f(k,\pi)|$ has started.) We can therefore conclude that for low Z scatterers on the range of k = 4–12 Å^{-1}, the total amplitude function can be approximated by a simple c/k^2 factor times an exponential term. The phase shift is also sufficiently linear in this range to justify neglect of the quadratic term. For higher Z scattering atoms, more complicated empirical functions will be needed, in order to account for the peaking in electron-atom scattering amplitude at higher energies. Furthermore, for better fits to the phase on wide ranges of data, extra nonlinear parameters will have to be introduced.

Also, the trend in exponential damping terms (from 0.010 for ferrocene to 0.028 for aqueous Co(II)) clearly shows the effect of bond strength on the fine structure amplitude. The fact that the thermal damping parameters increase as the metal–ligand bond strength decreases again suggests that our semiempirical functions actually have a physical foundation. Experimentally, it becomes evident that low temperature data collection will be essential to extending the energy range of observable fine structure.

The failure of our functional form for $k < 4.0$ Å^{-1} ($E_{\text{photoelectron}} < 61$ eV) is not surprising, for both the phase and amplitude of the backscattering function exhibit complicated behavior in the low energy regime. A large number of extra parameters would have to be introduced to obtain perfect correspondence with the observed fine structure, and structural information would be lost rather than gained by extra fitting because of parameter correlation. Correlation of fitting parameters exists because fine structure data were taken over a fairly limited range in k-space (typically discernible out to k = 12 Å^{-1} with low Z scatterers and the present signal-to-noise ratio). The phase and amplitude functions are not completely independent on such a limited range.

Nevertheless, over the range of k = 4–12 Å^{-1}, the fine structure can be approximated by a fairly simple function. Carbon, nitrogen, and oxygen appear to have smoothly decreasing backscattering amplitudes, and the total phase shifts are almost linear for these simple model compounds. This permits a significant reduction in the number of parameters used, and it permits the extension of curve fitting methods to multishell fits of x-ray absorption fine structure data for molecules such as metalloporphyrins.

Four-Shell Fits of Iron Tetraphenylporphyrins. The iron tetraphenylporphyrins give beautiful fine structure observable out to k = 12 Å^{-1}. The first derivative curves of the porphyrin data in the vicinity of the edge show that there are two inflection points in the steep rise (see Figure 1). The energy of the inflection point nearest the top of the steep rise was averaged from all the porphyrin data sets to give a value of 7126.3 eV, which was taken as the zero of photoelectron energy.

Several background subtraction schemes were tried for the porphyrins, involving fitting polynomials of various orders over various energy ranges. The analysis presented here compares the two schemes that gave the most consistent results. The simplest method to give consistent results was to subtract a third-order polynomial fitted to the log (I_0/I) data as a function of energy over the range 7200 eV to the end of the data set (typically 7725 eV). The second method was to subtract a third-order polynomial fitted over the range 7325 eV to the end

Table II. Results of Four-Shell Fit on Fe(TPP) Fine Structure Data[a]

Radial distance	$(2R + a_1)$, Å	R_{cryst}[b]	a_i[c] (Å)
Fe-N	3.148 (51)	1.971	−0.79
Fe-C_α	5.01 (15)	3.015	−1.02
Fe-C_γ	5.86 (15)	3.407	−0.96
Fe-C_β	7.35 (26)	4.233	−1.12

[a] The background was removed by fitting a third-order polynomial over the range of 7200–7725 eV and subtracting. The fit was done over the range of k = 4–12 Å^{-1}. [b] J. P. Collman, J. L. Hoard, N. Kim, G. Lang, and C. R. Reed, *J. Am. Chem. Soc.*, **97**, 2676 (1975). [c] Calculated by using the crystallographic distance and the values of $(2R + a_1)$ from the fit.

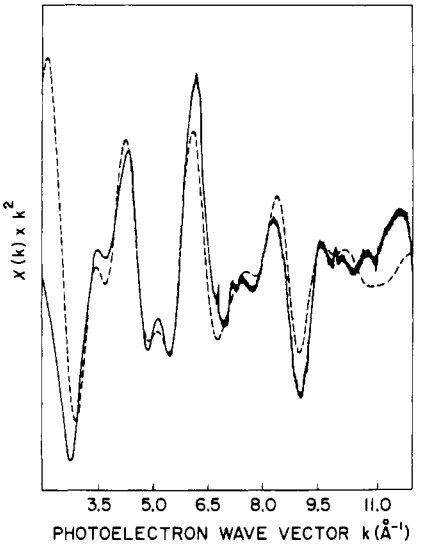

Figure 7. Four-shell fit (- - -) over the range of k = 4–12 Å^{-1} to the unfiltered fine structure data of Fe(TPP) (—). The fit used fixed values for the Debye-Waller factor, power on k in the amplitude function, and quadratic term, which were obtained from the single shell fits shown in Figure 6.

of the data set, then Fourier transform the data as a function of k over the k range 2–12 Å^{-1}, and transform back from the R range 0.5–7 Å.

Because of the molecular symmetry, each metalloporphyrin structure may be viewed as shells of scattering atoms grouped at equal distance from the central iron. The magnitude of the contribution to the fine structure decreases rapidly with increasing distance from the absorbing atom, so the absorption spectra of a compound such as Fe(TPP) may be approximated by the sum of four waves due to: (1) the coordinated nitrogens, (2) the α carbons (and axial imidazole α carbons if present), (3) the bridging γ carbons, and (4) the β carbons.

Each of the four waves has six constants to be determined: the amplitude C_i, the Debye-Waller factor $2\langle\sigma_i^2\rangle$, β_i (the power on k in the denominator of the amplitude function), and the three coefficients in the sine argument, a_{0i}, a_{1i}, and a_{2i}. Refining 24 constants in a four-shell fit would be next to meaningless. The results from single shell fits described earlier indicated that good choices for β, $2\langle\sigma_i^2\rangle$, and a_2 would be 2.0, 0.015, and 0.0, respectively for the range over which the fits were to be done. These values were held fixed in all fits of the porphyrin data thus reducing the number of variables to three per shell. A number of four-shell fits were done on Fe(TPP) using about 80 sample data points in each fit taken from the k range 4–12 Å^{-1}. The result of the Fe(TPP) fit is summarized in Table II. Figure 7 shows the agreement between observed and calculated spectra for this Fe(TPP) fit. Note that the

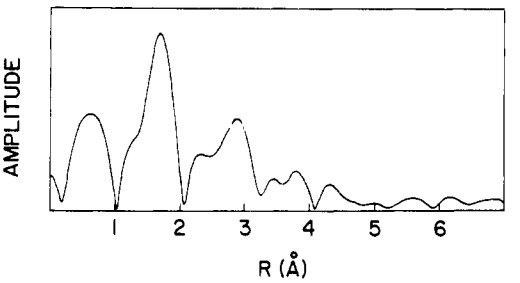

Figure 8. Fourier transform over the range of k = 4–12 Å^{-1} of the Fe(TPP) fine structure data. The first six peaks beyond R of 1 Å occur at 1.68, 2.30, 2.88, 3.44, 3.80, and 4.32 Å.

standard deviation of the $(2R + a_1)$ values increases substantially for the outer shells. The a_1 values, calculated by comparing $(2R + a_1)$ with the crystallographically determined R, are consistent for the three carbon shells to within one standard deviation. This consistency, as well as the overall goodness of fit, strongly suggests that the functional form used for the fit is valid. The starting values for C_1 and $(2R + a_1)$ for each wave were obtained from relative peak heights and peak positions in the Fourier transform of the respective data set.

For comparison with the results of the multishell fits, the Fourier transform of the Fe(TPP) data over the range of k = 4–12 Å^{-1} is shown in Figure 8. The main problem with the identification of peaks in the Fourier transform with values of $(2R + a_1)$ is that subsidiary "side lobes" may be expected for each main peak in the transform. For weaker, more distant shells there is confusion between a shell primary peak and a "side lobe" associated with a stronger shell. There is also the problem that skewing of the transformed envelope due to the nonlinear character of the phase and amplitude may artificially shift the value of the peak in $(2R + a_1)$.

At this point, it became apparent that the present range of data (and the theoretical understanding thereof) did not justify the inclusion of more parameters to simulate the experimental results. We thus embarked on a program of fine structure difference analysis, in which we hoped to correlate changes in EXAFS with well-defined changes in porphyrin structures.

Difference Fourier Analysis

Using the Fourier transform method, we have tried to detect the presence of axial ligands and measure the Fe to ligand distance in the iron porphyrin complexes. Unfortunately, with the present range of data, we cannot always directly resolve the axial ligand distance (for example, O_2, Cl^-, or $^-SC_6H_5$) from the iron porphyrin distances. With data recently acquired over a wider range in k space, this resolution has become possible.

Comparison of data from two similar compounds, however, can yield information about the structural differences between the two, assuming that the component backscattered waves from each neighboring atom are independent, and that the resultant fine structure is due to a simple sum of these waves. In the case of porphyrins, for example, if the Fe(TPP) data are appropriately subtracted from the data of an iron porphyrin which has axial ligands, the difference should be the fine structure from the axial ligands alone. But, often the structural differences between two iron tetraphenylporphyrins include the shift of the iron atom relative to the plane of the porphyrin, which lengthens the distance to each radial shell. If in-plane porphyrin fine structure is subtracted from the out-of-plane fine structure, the difference resembles the average of the two, but phase-shifted by about $\pi/2$ (since $(\sin x - \sin y)$ equals $2 \cos \frac{1}{2}(x + y) \sin \frac{1}{2}(x - y)$). Also contributing to the porphyrin-like appearance of the difference Fourier is the fact that it is difficult to scale the two data sets perfectly when sub-

tracting one from the other. When the difference in two porphyrins involves axial ligands as well as an out-of-plane shift, the difference in the fine structure will contain the sum of the two effects. Results from simulated data have shown that these effects may contribute equally to the difference transform. We refer to this Fourier transform of the difference of two data sets as a "difference Fourier".

The results of the difference Fourier for Fe(PPIX)Cl minus Fe(TPP) are shown in Figure 9. The one predominant peak in the difference Fourier is from the extra wave in the hemin chloride absorption spectrum which is due to backscattering by the chloride ion. More complicated difference Fouriers are obtained when there are axial ligands with more complicated structures. As mentioned before, this method is not without some pitfalls—a porphyrin-like (four or five wave) residual will be found in the difference Fourier if: (a) the scaling of the two data sets is incorrect, or (b) if a substantial change in iron porphyrin geometry occurs. Such a residual is observable to some extent in all the difference Fouriers.

A most interesting and useful difference Fourier (shown in Figure 10) is obtained from the comparison of fine structure of the oxy and deoxy forms of Fe($\alpha,\alpha,\alpha,\alpha$-TpivPP)(N-Me(imid)) data sets. Although there is a considerable background structure due to a change in the iron(II)-porphyrin distances, the primary components in the difference Fourier (first two significant peaks) correspond to the addition of a dioxygen ligand with two different iron-oxygen distances. The appropriate phase shifts (values of a_1) for Fe-O scattering are uncertain, so that calculation of absolute iron-oxygen distances is not possible. However, the *difference* between the two Fourier iron-oxygen peak positions should correspond to the *difference* between the distance of the Fe atoms to the bound oxygen, O, and the unbound oxygen, O′. The difference Fourier gives a value of (Fe-O) − (Fe-O′) of 1.0 Å. This difference compares extremely well with the crystallographically measured difference of 1.04 Å.[27] As expected, it can be seen that the peaks of 2.9, 3.6, 5.1, and 6.2 Å in the difference transform occur at values which are within about 0.1 Å of peaks in the straight Fourier transform of Fe(TPP) (compare Figures 8 and 10).

Because of the possible ambiguities associated with overlapping peaks in the difference Fourier transform and the possibility of nonlinear phase shift effects, fitting methods were used to further quantitate axial ligand distances and changes in iron-porphyrin geometry on ligation.

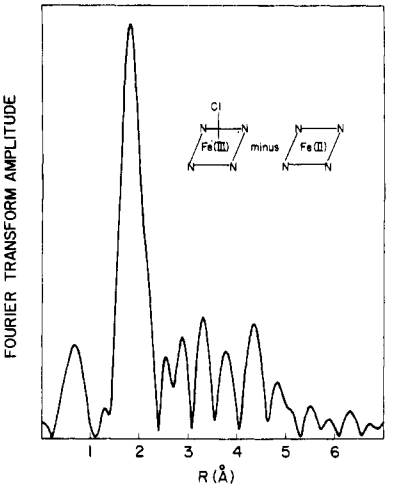

Figure 9. Difference Fourier transform over the range of k = 4-12 Å^{-1} for Fe(PPIX)Cl minus Fe(TPP) fine structure data. The peak at R of 1.78 Å which predominates results from the presence of the Cl ligand.

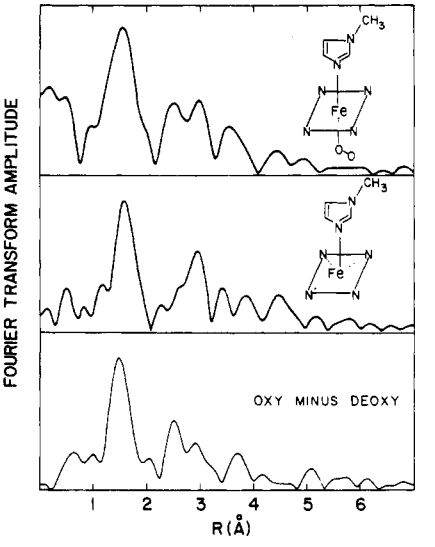

Figure 10. Fourier transforms (all over the range of k = 4-12 Å^{-1}) of oxy and deoxy Fe($\alpha,\alpha,\alpha,\alpha$-TpivPP)(N-Me(imid)) data. The upper transform shows the radial distribution for the oxy complex, and the middle transform for the deoxy complex. The lower difference transform was obtained by normalizing the data sets to one another and then transforming the difference. The peaks at 1.5 and 2.5 Å occur because of the presence of the asymmetrically bound dioxygen molecule.

Comparison Fit Analysis

In order to roughly determine the movement of the iron atom as it binds axial ligands, as well as to measure the iron to axial ligand distances, a procedure called comparison fitting was developed. Data from one of the two molecules being compared are fitted with a four-shell function as described earlier. The parameters from this fit which correspond to the three carbon shells in the porphyrin and the a_0 constant from the nitrogen shell are held fixed in fitting the data from the other molecule. Extra waves are added to account for axial ligands. The form of the function used to fit the second molecule is then:

$$\chi(k) = C_1 \frac{e^{-0.015k^2}}{k^2} \sin\,[a_0 + (2R + a_1)k] + C_2(\text{3 carbon shells}) + \text{extra waves}$$

C_1, $(2R + a_1)$, C_2, and the parameters in the extra waves are refined, and a_0 and the parameters in the three carbon shells, which come from the fit of the first molecule, are held fixed.

Two comparison fits were done using Fe(TPP) as the standard. Data from Fe(PPIX)Cl and Fe(TPP)(SC_6H_5) were both fit using the a_0 from the nitrogen shell and all the parameters from the three carbon shells from the four-wave fit of Fe(TPP), and adding one extra wave in each case. Comparison fits were also done on the Fe($\alpha,\alpha,\alpha,\alpha$-TpivPP)(N-Me(imid))$O_2$ data using parameters from the deoxy four-shell fit and adding two waves for the presence of the oxygen in the oxy data. Each fit was done on about 85 points over a k range of 4-12 Å^{-1}. As with the four-shell fits, the Debye-Waller factor, $(2\langle\sigma_i^2\rangle)$, the power on k, (β), and the quadratic coefficient in the phase, (a_2), were all held fixed at 0.015, 2, and 0, respectively.

In order to accurately measure an iron out-of-plane shift of 0.4 Å, the procedure must be able to detect accurately a difference of 0.08 Å in the nitrogen shell $(2R + a_1)$ value. The estimated standard deviation of this value is on the order of 0.06 Å in the preliminary four-shell fit and somewhat larger in the comparison fit itself, so that the calculated change in the iron-nitrogen distance using this procedure is more qualitative than quantitative. Further complicating the attempt at estimating the iron out-of-plane shift is the fact that this procedure assumes that the conformation of the porphyrin remains exactly the same from compound to compound, which may not

Table III. Results of Difference and Derivative Fits[a]

	Type of fit	Radial distance	$(2R + a_1)$ (Å)[b]	$R_{crystal}$ (Å)	a_1 (Å)[c]
Fe(PPIX)Cl	Difference	Fe-Cl	3.483 (40)	2.218[d]	−0.95
and Fe(TPP)	Derivative	Fe-Cl	3.483 (39)	2.218[d]	−0.95
Fe(TPP)(SC_6H_5)	Difference	Fe-S	3.45 (11)	2.32[e]	−1.19
and Fe(TPP)	Derivative	Fe-S	3.43 (08)	2.32[e]	−1.21
Oxy and Deoxy	Difference	Fe-O	3.03 (07)	1.75[f]	−0.47
Fe(α,α,α,α-TpivPP)		Fe-O′	5.05 (17)	2.79[g]	−0.53
(N-Me(imid))		(Fe-O′ − Fe-O)	1.01	1.04[g]	
	Derivative	Fe-O	3.03 (07)	1.75[f]	−0.47
		Fe-O′	5.05 (17)	2.79[g]	−0.53
		(Fe-O′ − Fe-O)	1.01	1.04[g]	

[a] Fits were all done over the range of k = 4–12 Å^{-1} using unfiltered data. [b] Estimated standard deviations are given in parentheses. [c] a_1 calculated for the appropriate radial distance using the crystallographic distance and values of $(2R + a_1)$. [d] D. F. Koenig, *Acta Crystallogr.*, **18**, 663 (1965). [e] Reference 27. [f] Reference 28. [g] Calculated from ref 28.

be the case if doming or other porphyrin distortions are involved. The $(2R + a_1)$ values are determined for the axial ligands in the extra waves. It is interesting, however, that out-of-plane shifts when calculated this way come close to the crystallographic results. For example, the calculated movement of the Fe atom relative to the porphyrin plane when going from Fe(TPP) to Fe(TPP)(SC_6H_5) is 0.40 Å and the crystallographic result for a similar compound Fe(TPP)($SC_6H_5NO_2$)[26] is 0.43 Å. This procedure was less promising than the methods using difference and derivative fits described below.

Difference and Derivative Fits

By directly comparing the fine structure of one iron porphyrin with that of a similar iron porphyrin containing additional axial ligands, the distance to these additional axial ligands can be accurately determined. To do this comparison, the fine structure data from the first porphyrin is fitted to that of the second. If the two data sets are scaled to each other in this manner, the difference between them is the fine structure due to the additional axial ligands. Fitting this difference with the fine structure functional form yields $(2R + a_1)$ values from which the distances to the axial ligands can be obtained, assuming values of a_1 are known. The functional form used for this "difference fit" is then:

$$\chi_2(k) = b_1\chi_1(k) + \sum_i \frac{C_i e^{-2(\sigma_i^2)k^2}}{k^{\beta_i}} \sin(2R_ik + a_{0i} + a_{1i}k + a_{2i}k^2)$$

where the sum is over the number of shells in the additional axial ligands. Starting values for the constants in the sum are obtained from a preliminary difference Fourier which is done without attempting to scale between the data sets. After the constant b_1 is determined from a difference fit, a final difference Fourier, in which the two data sets are appropriately scaled, gives a much better picture of the distances to axial ligands.

Problems sometimes occur with difference fits if the geometric changes between the two porphyrin molecules include a change in iron to porphyrin distance (an out-of-plane metal atom shift), since part of the difference is then a porphyrin-like spectrum. Since the change in metal–radial shell distances is responsible for this porphyrin-like difference, it would be desirable for the fitting function to account for this change as well as for the presence of extra axial ligands. An appropriate term to add to the fitting function would be derived from the first term of the Taylor series expansion as a function of R_i.

$$\sum_{i \text{ shells}} \Delta R_i(\partial\chi/\partial R_i)$$

where ΔR_i would be adjusted in the fitting procedure. We assume that the Debye–Waller factor is constant for small changes in R and that changes in inelastic scattering processes are negligible. Of course, the available data are a function of k not R. However, $\partial\chi/\partial R_i$ is related to $k(\partial\chi/\partial k)$ as shown in the following way.

First express χ as a function of k and R (leaving out the quadratic term in the sine argument):

$$\chi(k,R) = \sum \frac{A_i}{k^\beta R_i^2} \sin(2R_ik + a_0 + a_1k)$$

Then compare the partial derivatives with respect to R_i and k:

$$\sum_i \frac{\partial\chi}{\partial R_i} = \sum_i -\frac{2A_i}{k^\beta R_i^3} \sin(2R_ik + a_0 + a_1k) + \sum \frac{2A_i}{k^{\beta-1}R_i^2} \cos(2R_ik + a_0 + a_1k) \approx b\chi + \sum \frac{2A_i}{k^{\beta-1}R_i^2} \cos(2R_ik + a_0 + a_1k)$$

$$k\frac{\partial\chi}{\partial k} = k\left[\sum -\frac{\beta A_i}{k^{\beta+1}R_i^2} \sin(2R_ik + a_0 + a_1k) + \sum \frac{A_i(2R_i + a_1)}{k^\beta R_i^2} \cos(2R_ik + a_0 + a_1k)\right] \approx b'\chi + \sum \frac{A_i(2R_i + a_i)}{k^{\beta-1}R_i^2} \cos(2R_ik + a_0 + a_1k)$$

An appropriate fitting function that accounts for both the change in iron to porphyrin distances as well as the presence of additional axial ligands is then:

$$\chi_2 = b_1\chi_1 + b_2k\frac{\partial\chi}{\partial k} + \chi_{\text{additional ligand}}$$

The derivative with respect to k at each point of interest can be obtained numerically by fitting a polynomial to data around the point and differentiating the polynomial.

Difference and derivative fits were done on three different sets of data: Fe(PPIX)Cl minus Fe(TPP), Fe(TPP)(SC_6H_5) minus Fe(TPP), and oxy minus deoxy Fe(α,α,α,α-TpivPP)-(N-Me(imid)). These fits were typically done on about 85 sample points over the k range 4–12 Å^{-1}, and the results of these fits are shown in Table III. There also appeared to be very little difference in numerical results obtained from derivative and difference fits done over the same range using filtered and unfiltered data.

The derivative and difference fits give very consistent and accurate results when used for predicting distances to axial ligands. For example, the derivative fit on the deoxy and oxy forms of Fe(α,α,α,α-TpivPP)(N-Me(imid)) is shown in Figure

11. The quality of the fit obtained by the addition of the derivative term and the contribution of the oxygen can be seen by comparing the upper two curves (oxy and deoxy) with the lower two curves in which the oxy data have been simulated by adding in the contribution due to the additional oxygen and the derivative term. The derivative fit gives a ΔR value ($R_{Fe-O} - R_{Fe-O'}$) of 1.01 Å with an estimated standard deviation of 0.03 Å for R_{Fe-O} and 0.08 Å for $R_{Fe-O'}$. This ΔR value compares very well with the crystallographic distance of 1.04 Å.[27] The ratio of the weights of the two oxygen waves (b_1(Fe-O')/b_1(FeO)) comes out somewhat higher (59%) than is predicted by the inverse square law (41%) of the functional form of EXAFS which was given earlier. This suggests that at the current level of semiempirical representation the relative weight may be used to give only a rough (40% or so) estimate of coordination numbers.

In principle, it should also be possible to extract accurate information about the change in the Fe–N distance (as well as the axial ligand distances) from the derivative fits. From the earlier discussion, it can be seen that the term $b_2k(\partial\chi/\partial R)$ represents the second term in the Taylor series expansion of χ as a function of R. In some cases, subsequent terms in the expansion are not insignificant compared to this term so the magnitude of b_2 is not always a good measure of the magnitude of the out-of-plane shift. However, in most cases examined thus far the sign of b_2 correctly predicts the direction of the shift, whether in or out of the plane. Including the b_2 term when an iron atom shift is involved does substantially improve the fit over a difference fit, and thereby reduces the standard deviations of the parameters.

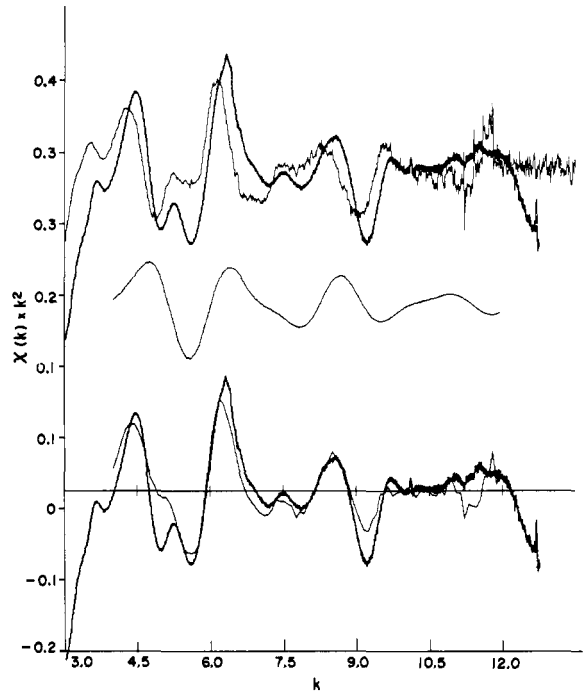

Figure 11. The effect of derivative fits (over the range of k = 4–12 Å^{-1}), the simulation of the oxy Fe($\alpha,\alpha,\alpha,\alpha$-TpivPP)(N-Me(imid)) spectrum from the deoxy spectrum plus oxygen waves and the derivative term. The upper two curves compare directly the oxy (- - -) and deoxy (—) fine structure data. The middle curve is the contribution to be added to the deoxy data (containing the two oxygen waves and the derivative) in order to simulate the oxy data. The lower curves show a comparison of the oxy data (- - -) with the data obtained by combining the deoxy fine structure with the derivative and oxygen contribution (middle curve).

Discussion and Conclusions

We have reported the development of a semiempirical functional form to describe extended x-ray absorption fine structure spectra and have used this form for the interpretation of spectra from organometallic complexes using curve fitting techniques. The results described in this paper support the essential correctness of this approach and establish that it is a valuable alternative to the Fourier transform method of analysis. Extrapolation from the single shell fits to the multishell porphyrin fits shows that under certain conditions the fine structure contributions from different atoms are additive.

Curve fitting showed that a simple model for the fine structure amplitude ($1/k^\beta$, where values of ranged from 1.7 to 2.2) gave values somewhat lower than the value of 3 expected from the Born approximation in the high k limit. Although not necessarily significant, the falloff of the fine structure amplitude function is slower with oxygen than with nitrogen, which is in turn slower than with carbon. While the total fine structure amplitude for these light elements can be successfully modeled by a simple function (an inverse power of k times an exponential), such is not expected to be the case for high Z elements in which the backscattering amplitude peaks at higher photoelectron energies.[29] The shape of the backscattering amplitude is characteristic of the type of backscattering atom and its bonding. Such behavior may be diagnostic for the identification of specific environments of the absorbing atom. A bound sulfur atom should be distinguishable from oxygen or nitrogen, and metal–metal interactions will also be readily observable (since the amplitude will peak at a much higher energy). Thus the amplitude as well as the phase will be important for the interpretation of the extended fine structure of metalloproteins.

We have shown that while it is difficult to get precise structural information (better than 0.1 Å) from a single EXAFS spectrum of a complex molecule, it *is* possible to get very accurate information on structural changes. We have developed new methods of the difference fitting analysis which readily provide much more accurate information when looking at structural changes around the absorbing metal ion.

From the expression ($2R + a_1$) which is varied in the fitting routines, it has been shown that reasonably accurate distances can be obtained if the value of a_1 is known. From the results of our fits on a variety of iron porphyrins, we have determined that reasonable values of a_1 in these compounds[30] are −0.95, −1.2, −0.47, −0.79, and −1.0 Å for S, Cl, O, N, and C, respectively. These a_1 values appear to be reasonably independent of the chemical environment, and transferrable from molecule to molecule.[31] For example, using the Fourier transform a_1 value of 1.12 Å determined by Sayers, Stern, and Herriott[32] for Fe–S scattering in FeS_2 and the ($2R + a_1$) value of 3.43 Å from the average of our difference and derivative fit results for Fe(TPP)(SC_6H_5) − Fe(TPP) (see Table III), we calculated an Fe–S distance in Fe(TPP)(SC_6H_5) of 2.31 (4) Å. The crystallographic distance in a very similar compound Fe(PPIX)(SC_6H_5-NO_2) is 2.32 (1) Å.[27]

It has also been shown that the difference analysis methods can distinguish between various modes of ligand binding (within the limits of radial distribution). In the case of the oxy form of Fe($\alpha,\alpha,\alpha,\alpha$-TpivPP)(N-Me(imid)), for example, the difference Fourier showed two peaks (at 1.5 and 2.5 Å) indicative of binding of the Fe to dioxygen in the "end-on" or Pauling manner. Should symmetrical π bonding have been the case, only one peak, intermediate in distance between the two, would have been observed. (Likewise, the derivative fits would have required only one additional wave with twice the weight to describe the oxy spectrum in terms of the deoxy.) While, in principle, the magnitude of the derivative can be used to extract changes in the distances from the Fe to the porphyrin atoms, the series termination effects mentioned earlier prevented this.

$$\begin{array}{ccccccc}
\frac{-V_2}{|V_{12}|} & \frac{V_1}{|V_{12}|} & 0 & 0 & 0 & \cdots & 0 \\
\frac{-V_1\ V_3}{|V_{12}||V_{123}|} & \frac{-V_2\ V_3}{|V_{12}||V_{123}|} & \frac{|V_{12}|}{|V_{1234}|} & 0 & 0 & \cdots & 0 \\
\frac{-V_1\ V_4}{|V_{123}||V_{1234}|} & \frac{-V_2\ V_4}{|V_{123}||V_{1234}|} & \frac{-V_3\ V_4}{|V_{123}||V_{1234}|} & \frac{|V_{123}|}{|V_{1234}|} & 0 & \cdots & 0 \\
\frac{-V_1\ V_5}{|V_{1234}||V_{12345}|} & \frac{-V_2\ V_5}{|V_{1234}||V_{12345}|} & \frac{-V_3\ V_5}{|V_{1234}||V_{12345}|} & \frac{-V_4\ V_5}{|V_{1234}||V_{12345}|} & \frac{|V_{1234}|}{|V_{12345}|} & \cdots & 0 \\
\vdots & \vdots & \vdots & \vdots & \vdots & & \vdots \\
\frac{V_1}{|V_{12\ldots n}|} & \frac{V_2}{|V_{12\ldots n}|} & \frac{V_3}{|V_{12\ldots n}|} & \frac{V_4}{|V_{12\ldots n}|} & \frac{V_5}{|V_{12\ldots n}|} & \cdots & \frac{V_n}{|V_{12\ldots n}|}
\end{array} \qquad \text{(I)}$$

While not discussed in this paper, x-ray photoabsorption spectroscopy can give other kinds of information about the absorbing metal ion. The absolute position of the absorption edge gives information about the effective coordination charge on the absorbing metal ion.[33] Our work on edge shapes has recently suggested that the shape of the absorption edge (as determined by the presence of various bound states, as well as the ionization transitions) is sensitive to changes in the type of ligating atom. It should be possible, for example, based on edge shapes alone to distinguish an axial sulfur ligand from an axial nitrogen ligand in an iron porphyrin. These results will be discussed in detail in a future communication; however, it can be seen that this information, along with the structural results obtainable as described herein, makes x-ray photoabsorption spectroscopy a powerful technique for the study of organometallic structure.

It thus appears that x-ray photoabsorption spectroscopy will provide a complimentary technique to other analysis methods by providing direct distance information resulting from structural changes in the local environment of a selected metal ion in a complex macromolecule. The applications of such a methodology span the areas from study of heterogeneous catalysts to study of superconducting organometallics. Perhaps some of the most significant information may come from investigation of enzymatic and metalloprotein systems where changes in substrate metal interactions are critical to the function of the physiological process. Work in these areas is being pursued.

Acknowledgments. We would like to thank Tom Sorrell for his generous assistance in synthesizing a number of the porphyrin samples used in this study, and Dr. Susan Hayes for her preparation of the "oxy-picket fence". We thank Dr. B. Kincaid for his helpful comments on this work. We would also like to acknowledge the help of Herman Winick and the other members of the Stanford Synchrotron Radiation Project Staff for their technical assistance in support of this project. This work was partially supported by the donors of the Petroleum Research Fund, administered by the American Chemical Society, and by the Stanford Synchrotron Radiation Project supported by the National Science Foundation Grant DMR 73-07692-A02 in cooperation with the Stanford Linear Accelerator Center and the Energy Research and Development Administration.

Appendix

Numerical Analysis Methods. Least absolute value (rather than least squares) fits were done by minimizing the function

$$G = \sum_{i=1}^{N} k^3 |\chi_i - F_i|$$

where N is the number of data points fit, k is the wave vector, χ_i is the ith data point, and F_i is the value of the fitting function. The minimizations were done by a general minimization program using an algorithm somewhat similar to that of Rosenbrock[24] in which no derivatives are required. Each minimization step consisted of searching out a minimum in n directions one at a time, n being the number of adjustable parameters. At the end of each step, the n orthogonal directions of search were rotated such that the last direction of search in any step was in the overall direction taken by the previous step. The directions of search are given by the row vectors in the matrix shown in (I) where $V_1, V_2, V_3, \ldots, V_n$ is the vector of the overall direction of the previous step, and $|V_{12}| = \sqrt{V_1^2 + V_2^2}$, $|V_{23}| = \sqrt{V_1^2 + V_2^2 + V_3^2}$, etc. The distance that the program searched in each direction was decreased as the fit improved until it reached 10^{-12} and the program halted. The program required initial guesses at the parameters which were then refined.

References and Notes

(1) (a) A. Robinson, *Science*, **190**, 1074 (1975); (b) W. Metz and A. Robinson, *ibid.*, **190**, 1186 (1975).
(2) L. I. Schiff, "Quantum Mechanics", 3d ed, McGraw-Hill, New York, N.Y., 1968, pp 420–423.
(3) For a review of x-ray absorption spectroscopy, see L. Azaroff and D. Pease in "X-ray Spectroscopy", L. Azaroff, Ed., McGraw-Hill, New York, N.Y., 1974, Chapter 5. For a review of the older extended fine structure theories, see L. V. Azaroff, *Rev. Mod. Phys.*, **35**, 1012 (1963).
(4) B. M. Kincaid, P. M. Eisenberger, K. O. Hodgson, and S. Doniach, *Proc. Natl. Acad. Sci. U.S.A.*, **72**, 2340 (1975).
(5) R. de l. Kronig, *Z. Phys.*, **70**, 317 (1931); **75**, 191, 468 (1932).
(6) (a) C. A. Ashley and S. Doniach, *Phys. Rev. B*, **11**, 1279 (1975); (b) A. I. Kostarev, *Zh. Eksp. Teor. Fiz.*, **19**, 413 (1949); (c) H. Petersen, *Z. Phys.*, **98**, 569 (1936); (d) T. Shiraiwa, T. Ishimura, and M. Sawada, *J. Phys. Soc. Jpn.*, **13**, 847 (1958); (e) A. I. Kozlenkov, *Bull. Acad. Sci. USSR, Phys. Sci. (Engl. Trans.)* **25**, 968 (1961).
(7) P. A. Lee and J. B. Pendry, *Phys. Rev. B*, **11**, 1279 (1975).
(8) (a) E. A. Stern, *Phys. Rev. B*, **10**, 3027 (1974); (b) D. E. Sayers, Ph.D. Thesis, University of Washington, Seattle, Wash., 1971.
(9) B. Kincaid and P. Eisenberger, *Phys. Rev. Lett.*, **34**, 1361 (1975).
(10) D. E. Sayers, F. W. Lytle, and E. A. Stern, *Adv. X-Ray Anal.*, **13**, 248 (1970).
(11) (a) D. E. Sayers, F. W. Lytle, M. Weissbluth, and P. Pianetta, *J. Chem. Phys.*, **62**, 2514 (1975); (b) F. W. Lytle, D. E. Sayers, and E. A. Stern, *Phys. Rev. B*, **11**, 4825 (1975); (c) E. A. Stern, D. E. Sayers, and F. W. Lytle, *ibid.*, **11**, 4836 (1975).
(12) R. G. Shulman, P. Eisenberger, W. E. Blumberg, and N. A. Stambaugh, *Proc. Natl. Acad. Sci. U.S.A.*, **72**, 4003 (1975).
(13) J. P. Collman, J. L. Hoard, N. Kim, G. Land, and C. A. Reed, *J. Am. Chem. Soc.*, **97**, 2676 (1975).
(14) J. P. Collman and C. A. Reed, *J. Am. Chem. Soc.*, **95**, 2048 (1973).
(15) L. M. Epstein, D. K. Straub, and C. Maricondi, *Inorg. Chem.*, **6**, 1720 (1967).
(16) J. P. Collman, T. N. Sorrell, and B. M. Hoffman, *J. Am. Chem. Soc.*, **97**, 913 (1975).
(17) J. P. Collman, R. R. Gagne, C. A. Reed, T. R. Halbert, G. Lang, and W. T. Robinson, *J. Am. Chem. Soc.*, **97**, 1427 (1975).
(18) W. L. Jolly, "The Synthesis and Identification of Inorganic Compounds", Prentice-Hall, Englewood Cliffs, N.J., 1970, p 484.
(19) J. Bjerrum and J. P. McReynolds, *Inorg. Syn.*, **2**, 217 (1946).
(20) H. Winick in "Proceedings of the Ninth International Conference on High Energy Accelerators", Stanford Linear Accelerator Center, Stanford, Calif., 1974, pp 685–688.
(21) B. Kincaid, P. Eisenberger, and D. Sayers, *Phys. Rev.*, submitted for publication.

(22) Although the incident photon energy is high, the total number of photons absorbed is very small compared to the number of molecules present. Under typical conditions, at 7 KeV the flux is on the order of 10^8 photons/s with a bandwidth of about 1 eV.
(23) See Appendix section for a brief description of the numerical methods.
(24) H. H. Rosenbrock, *Comput. J.*, **3**, 175 (1960).
(25) Actually the extended fine structure is defined as $(\mu - \mu_0)/\mu_0$, where μ is the observed absorption coefficient and μ_0 is that of the free atom. However, if μ_0 changes slowly on the given energy range, the subtraction procedure will be correct to within a normalization factor.
(26) B. Kincaid, Ph.D. Thesis, Stanford University, Stanford, Calif., 1975.
(27) J. Koch, S. C. Tang, R. H. Holm, R. B. Frankel, and J. A. Ibers, *J. Am. Chem. Soc.*, **97**, 916 (1975).
(28) J. P. Collman, R. R. Gagne, C. A. Reed, W. T. Robinson, and G. A. Rodley, *Proc. Natl. Acad. Sci. U.S.A.*, **71**, 1326 (1974).
(29) The amplitude modulation of the observed fine structure is discussed in ref 26, p 89 and ref 11b, p 2832.
(30) The values of a_1 were derived from compounds where Fe was the absorbing atom. The numerical fits were done over a k range of 4–12 $Å^{-1}$.
(31) Further test of such transferrability has recently been made by B. Kincaid, P. Citrin, and P. Eisenberger, *Phys. Rev.*, submitted for publication.
(32) D. E. Sayers, E. A. Stern, and J. R. Herriott, *J. Chem. Phys.*, in press.
(33) S. P. Cramer, T. K. Eccles, F. W. Kutzler, K. O. Hodgson, and L. E. Mortenson, *J. Am. Chem. Soc.*, **98**, 1287 (1976).

Crystal Structure, Raman Spectrum, and Nuclear Magnetic Resonance Spectrum of Methoxythionyl μ-Fluoro-bis(pentafluoroantimonate(V)), $CH_3OSO^+Sb_2F_{11}^-$

R. J. Gillespie,* F. G. Riddell, and D. R. Slim

Contribution from the Department of Chemistry, McMaster University, Hamilton, Ontario, Canada. *Received June 18, 1976*

Abstract: The compound $CH_3OSO^+Sb_2F_{11}^-$ has been prepared by the reaction of methyl fluoride with antimony pentafluoride in liquid sulfur dioxide. Its structure has been investigated by ^{19}F spectroscopy of its solutions in SO_2, by Raman spectroscopy of the polycrystalline solid, and by an x-ray crystallographic examination of a single crystal. The crystals are triclinic with $a = 5.391$ (5), $b = 8.059$ (3), $c = 13.932$ (4) Å, $\alpha = 90.63$ (4), $\beta = 102.12$ (5), $\gamma = 102.62$ (2)°. The structure was refined in the space group $P\bar{1}$ to a final agreement index of 0.0420 for 1405 independent reflections. The structure is made up of discrete CH_3OSO^+ cations and linear $Sb_2F_{11}^-$ anions.

Solutions of CH_3F and SbF_5 in sulfur dioxide and in sulfuryl chlorofluoride have long been thought to contain one or more CH_3F–SbF_5 complexes for which various formulations have been given.[1,2] However, the absence of H–F coupling in the ^1H and ^{19}F NMR spectra of these solutions has long remained an unexplained difficulty. Very recently Peterson et al.[3] reported the preparation of a white crystalline compound from the reaction of a 1:1 mixture of SbF_5 and CH_3F with SO_2 in solution in SO_2ClF. Because the compound reacted with methanol and ethanol to give dimethyl sulfite and methyl ethyl sulfite, respectively, rather than dimethyl ether and methyl ethyl ether, as reported previously,[1] Peterson proposed that the compound was $CH_3OSO^+SbF_6^-$ (or $Sb_2F_{11}^-$), in which, of course, no H–F coupling is expected.

At the same time Olah et al.[4] reinterpreted their earlier NMR data in terms of the formation of CH_3OSO^+ in SO_2 solution and $CH_3OSOClF^+$ in SO_2ClF solution. He has also shown by the observation of the expected H–F coupling in the ^1H NMR spectrum in SO_2F_2 as solvent, that the CH_3F–SbF_5 complex is formed in this solvent which, unlike SO_2 and SO_2ClF, is not methylated.

In this paper we report the isolation of a white crystalline compound from a solution of CH_3F and SbF_5 in SO_2, which is presumably the same compound as was reported by Peterson et al.[3] and also mentioned briefly by Olah et al.[4] Investigation of this compound by x-ray crystallography, Raman spectroscopy, and ^1H and ^{19}F NMR spectroscopy has shown that it is indeed not a CH_3F–SbF_5 complex but is the compound $CH_3OSO^+Sb_2F_{11}^-$.

Experimental Section

Antimony pentafluoride (Ozark-Mahoning) was purified by a double distillation in an all glass apparatus and sulfur dioxide (Matheson) was repeatedly distilled from, and kept over, phosphorus pentoxide before use. Methyl fluoride (Peninsular Chemical Research) was not further purified.

In a typical experiment, SbF_5 (5×10^{-3} mol) was syringed into one arm of a rigorously dried Pyrex glass double ampule inside a drybox. The apparatus was connected to the vacuum line and methyl fluoride (2.5×10^{-3} mol) and sulfur dioxide (2×10^{-2} mol) were condensed onto the SbF_5 at −196 °C. The mixture was allowed to warm to −78 °C and was stirred at this temperature for about 30 min. The mixture was allowed to warm up to −7 °C and the solvent was then removed by cooling the other ampule to −30 °C. White crystals were left behind and were pumped to dryness. Suitable crystals for x-ray studies were mounted in thin-walled quartz capillaries inside a drybox equipped with a microscope.

Crystal Data. $CH_3OSO^+Sb_2F_{11}^-$ is triclinic with $a = 5.391$ (5), $b = 8.059$ (3), $c = 13.932$ (4) Å, $\alpha = 90.63$ (4), $\beta = 102.12$ (3), $\gamma = 102.62$ (1)°, $V = 576$ Å^3, $Z = 2$, $D_c = 3.06$, fw = 531.4, $F(0,0,0) = 488$, $\lambda(\text{Mo K}\bar{\alpha}) = 0.71069$ Å, and $\mu(\text{Mo K}\alpha) = 51$ cm^{-1}. The unit cell parameters were obtained from a least-squares refinement of 15 reflections in the region $20° < 2\theta < 25°$. The structure was successfully refined in the centrosymmetric space group $P\bar{1}$. (Ci,[5] No. 2).

X-Ray Intensity Measurements. The crystal, which was an irregular block of approximate dimensions $0.28 \times 0.16 \times 0.09$ mm, was sealed in a thin-walled quartz capillary and mounted on a Syntex $P\bar{1}$ diffractometer with its 0.28-mm edge, which was approximately perpendicular to the (1,0,0) face, almost coincident with the ϕ axis of the diffractometer. Intensities were measured using graphite monochromated Mo K$\bar{\alpha}$ radiation, with a θ–2θ scan and a scan rate varying from 8.0 to 24.0°/min in 2θ so that weaker reflections were examined more slowly to minimize counting errors. Stationary background counts, with a time equal to half the scan time for each reflection, were made at each end of the scan range. The scan width varied from 2° at low 2θ to 2.5° for high-angle reflections. One standard reflection was regularly checked to monitor the stability of the crystal and its alignment, but no significant variation was observed. Independent reflections (1405) within the range $2\theta < 50°$ were measured resulting in 1331 reflections with intensities greater than three times their